Scale Effect on Liquid Film Formation in a Prefilming Type Air-blast Atomizer

Mitsunori Itoh*[1], Shinsuke Matsuno[1]
[1] Research Laboratory, IHI Corporation, Japan
* Corresponding author: mitsunori_itou@ihi.co.jp

Abstract
Aiming at a contribution to improve the liquid film formation in the prefilming type air-blast atomizer, this study focuses on the wetting behavior of the finite-width liquid rivulet on the solid surface under the condition of strong shear stress of the air. The stretching motion of the liquid film is theoretically modeled in the study on the basis of minimal energy concept which predicts the breakup of the liquid film. The motion of the liquid film is analytically predicted and experimentally validated. As a result, the theoretical model well predicts the wetting motion of the liquid in much larger liquid flow rate condition, in other wards much larger liquid film width condition. On the other hand, the motion of the liquid film does not agree with the theoretically predicted one in smaller liquid film width condition. This is because the liquid flow cannot changes its shape freely at the minimal energy status but its shape is geometrically confined by the surface tension force in a surface tension force-dominant condition due to the small length scale of the liquid. The confined shape model is theoretically constructed on the basis of the confined shape concept and compared to the experimental result. As a result, better agreement is observed in smaller length condition.

Introduction
Air-blast atomizer [1] utilized in aero-engine or gasturbine combustors atomizes liquid fuel by utilizing the momentum of combustion air that is fed into combustion chamber. In general, the atomizing air is given swirl in the atomizer nozzle by swirl vane and the swirl flow stabilizes flames of the fuel spray in front of the nozzle exit by recirculation of the swirl flow. In contrast to pressure atomizers [1] that control the atomization by the momentum of the fuel itself, the momentum of the atomizing air and causal behavior of the liquid fuel are the influencing factors to decide the condition of the fuel spray. It is said that the characteristic length scale of the liquid before atomization affects the droplet diameter of the spray [2-3]. In prefilming type air-blast atomizers, the liquid fuel is fed onto the prefilmer surface and thinned to be a film-like shape, giving the conditions of subsequent atomization process. In this type atomizer, the thickness of the liquid film is the key length scale to characterize the spray [4]. In practical engine operations, the condition of the air such as velocity, flow rate and momentum is uniquely given in each operating status. Under the fixed air condition, it is possible to reduce the thickness of the liquid film by decreasing the flow rate of the liquid film per unit surface area of prefilmer. Thinning the film gives finer spray condition; on the other hand, it also enhances the possibility of breakup of the liquid film that causes the decay of the spray quality. In practical aero-engine operation, the fuel flow rate varies significantly in each operating stage such as idle, takeoff or cruise. Furthermore, the condition of the air also varies largely in each stage. Hence it is necessary to control the liquid film condition in a large variety of the fuel and the air condition. In previous researches, the wetting behavior of the liquid film is well studied in not only aero-engine application but also various industrial ones. The motion of the two dimensional liquid film that assumes the perfectly wetting condition was theoretically modeled. On the other hand, the studies focusing on the motion of the finite-width liquid film with contact line near its edge, especially under the condition of strong shear stress affecting, is not so many, as far as the authors know. This study focuses on the wetting behavior of the finite-width liquid rivulet on the solid surface under the condition of strong shear stress of the air. In this study, the stretching motion of the liquid film is theoretically modeled on the basis of minimal energy concept [5] which predicts the breakup of the liquid film. The motion of the liquid film is analytically predicted and experimentally validated. The analysis assumes the rectangle cross section and the Cuette flow velocity profile in liquid flow for simplicity. On the other hand, the surface of the liquid film is deformed as a result of balance of the surface tension force and the shear stress of the air. Hence, the actual wetting motion of the liquid film is expected to have some difference from theoretical one due to the deformation by the surface tension force. The effect of the surface tension force is characterized by the length scale. The purpose of this study is to obtain the validity of the model assumption and the effect of the length scale on it.

Theoretical model

When designing the air-blast atomizer, the flow rate of the liquid and the momentum (velocity and density) of the air are given in each operating status of the engine. The motion of the liquid film with finite width should be modeled theoretically from these given values. Here, velocity, thickness and width of the liquid film are the values to be specified in the model. Figure 1 shows the modeled motion of the liquid film. The model assumes the steady Cuette flow profile [6] in flow-wise cross section for simplicity. The velocity of the liquid is assumed to be much smaller than that of the air. The liquid film is stretched by the shear force of the air and has a rectangle shape in with large aspect (width to thickness) ratio in span-wise cross section. The velocity of the liquid along span-wise direction is assumed to be uniform. In practical, the liquid film has some deformation [7] or the instability [8] caused by the surface tension force as shown in Fig. 1. However, these effects are neglected for simplicity.

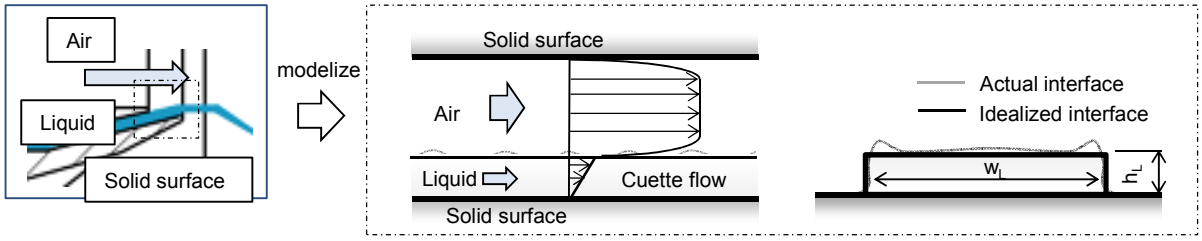

Figure 1. Modeled motion of liquid film

Based on above assumptions, the mass and the momentum conservation equations are respectively obtained as Eq 1 and Eq. 2.

$$Q_L = \frac{1}{2} u_{L,s} w_L h_L \tag{1}$$

$$c_f \frac{1}{2} \rho_a u_a^{\,2} = \mu_L \frac{u_{L.s}}{h_L} \tag{2}$$

In two dimensional problem, the flow rate of the liquid is given as the flow rate per unite surface width. Therefore, two unknown values, i.e. the thickness and the velocity of the liquid, are determined from above two equations. In finite-width problem, however, the width of the liquid film is added as the unknown quantity to be specified. Hence the one more equation is needed for specifying the three unknown quantities. Here the minimal energy concept of the liquid film is considered. The liquid film is stretched by the work from the air flow and extends its surface area. Therefore, the shape and the motion of the liquid film becomes stable under the condition on which the total energy that the liquid film gains from the air becomes the minimum. In the research concerning the micro contactor, Monnier et al. analyzed the motion of falling liquid film in channels by gravity force [5]. In our analytical approach, the shear stress of the air is considered as a driving force. The total energy per width (span-wise length) that the liquid film gains is the sum of the kinetic, potential and surface energy, shown in Eq. 3.

$$\varepsilon_{total} = \varepsilon_k + \varepsilon_{st} + \varepsilon_p \tag{3}$$

The kinetic energy per unit width is represented as Eq. 4.

$$\varepsilon_k = \int_{-\frac{w_L}{2}}^{\frac{w_L}{2}} \int_0^{h_L} \frac{1}{2} \rho_L u_L^{\,2} dy dx \tag{4}$$

The cross sectional shape of the liquid film is assumed to be rectangle with large width to thickness ratio. Therefore, the thickness-wise surface energy is ignored and the two interfaces of liquid-gas and liquid-solid are assumed to be the same as each other and as the width of the liquid film. Based on this assumption, the surface energy per unit width is represented as Eq. 5 [9].

$$\varepsilon_{st} = \left(\sigma_{LV} + \sigma_{LS} - \sigma_{SV}\right) w_L \tag{5}$$

Here, the equilibrium of the surface tension force of each phase is represented in Eq. 6.

$$\sigma_{SV} - (\sigma_{LS} + \sigma_{LV} \cos\theta_{CA}) = 0 \tag{6}$$

By substituting Eq. 6 into Eq. 5, the surface energy is obtained as Eq. 7.

$$\varepsilon_{st} = \sigma_{LS}(1 - \cos\theta_{CA}) w_L \tag{7}$$

The potential energy is represented in Eq. 8.

$$\varepsilon_p = \rho_L g_p h_L w_L \frac{1}{2} L \tag{8}$$

Here, g_p is acceleration. The gravity or centrifugal force corresponds to this value. L is the length of the liquid film parallel to the potential direction. This value varies with the attitude of the apparatus. The potential force is ignored in below section because of its smallness compared to other forces. Figure 2 shows the energies that the liquid film gains under the arbitrarily selected condition. Both the kinetic and surface energies are calculated from Eq. 4 and Eq. 7, respectively. Total energy is the sum of both energies. When calculating these energies, the thickness-width ratio of the liquid film is changed arbitrarily as a parameter under the regulation defined by Eq. 1 and Eq. 2. The horizontal axis of the figure is the width of the liquid film and vertical one is the energies. The kinetic energies and the causal total energies in three different air conditions are shown in the figure. The surface energy is independent of the air velocity, so that the only single result is shown.

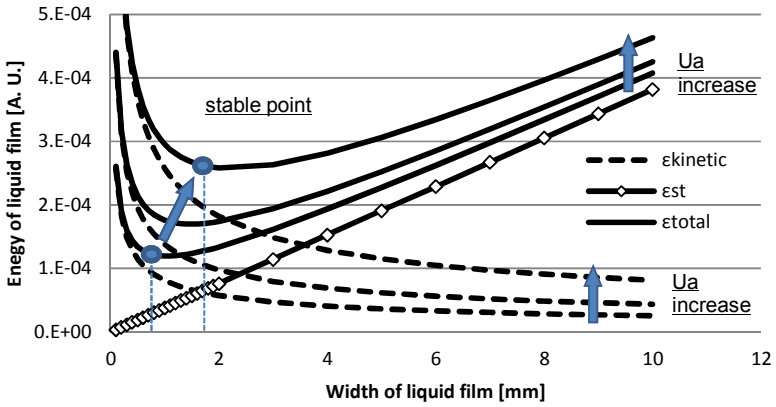

Figure 2. Relationship between liquid film width and energies

As can be seen in the figure, the kinetic energy uniformly decreases with increasing film width. This is because increasing film width is equal to the decreasing film thickness under the definition of the mass conservation. Therefore, decreasing thickness causes the decrease of the kinetic energy under the assumption of the Cuette flow; the velocity gradient of the liquid film is kept constant but the velocity itself becomes larger with increasing film thickness in fixed air velocity and liquid flow rate condition. On the other hand, the surface energy linearly increases with increasing film width because the surface energy is proportional to the width. As a result, the sum of both two energies is concave up and has extreme value in a point of the film width. In practical, the width and any other behavior of the liquid film are assumed to be determined at the minimal energy condition. The minimal energy condition shifts toward larger width condition with increasing air velocity. The minimum energy condition of the liquid film is mathematically determined as Eq. 9.

$$\frac{d\varepsilon_{total}}{dw_L} = 0 \tag{9}$$

From the discussion above, the three unknown quantities of the liquid film are specified from Eq. 1, Eq. 2 and Eq. 9. By equating these three equations, width, thickness and the velocity of the liquid film to describe the motion are obtained from Eq. 10, Eq. 11 and Eq. 12.

$$W_L = \left\{ \frac{\rho_L^2 \tau_a}{18\sigma_{LS}^2 \mu_L (1 - \cos\theta_{CA})^2} \right\}^{\frac{1}{3}} Q_L \tag{10}$$

$$h_L = \left\{ \frac{\rho_L \tau_a}{12\sigma_{LS}\mu_L^2 (1 - \cos\theta_{CA})} \right\}^{\frac{1}{3}} \quad (11)$$

$$u_{L,s} = \left\{ \frac{\rho_L \mu_L}{12\tau_a \sigma_{LS} (1 - \cos\theta_{CA})} \right\}^{\frac{1}{3}} \quad (12)$$

Here, the shear stress of the air is obtained from Eq. 13.

$$\tau_a = c_f \frac{1}{2} \rho_a u_a^2 \quad (13)$$

As a result, the thickness and the velocity of the liquid film are determined by the air condition and independent of the flow rate of the liquid as shown in Eq. 10 and Eq. 11. On the other hand, the width of the liquid film proportionally increases with liquid flow rate as shown in Eq. 12. Our analytical approach is based on the concept of the minimal energy and the modelization of the shear stress of the air as a driving force. The analysis assumes the rectangle cross section and the Cuette flow velocity profile in liquid flow for simplicity. The analytical equations obtained from the above assumptions are to be validated experimentally in below sections.

Experimental setup

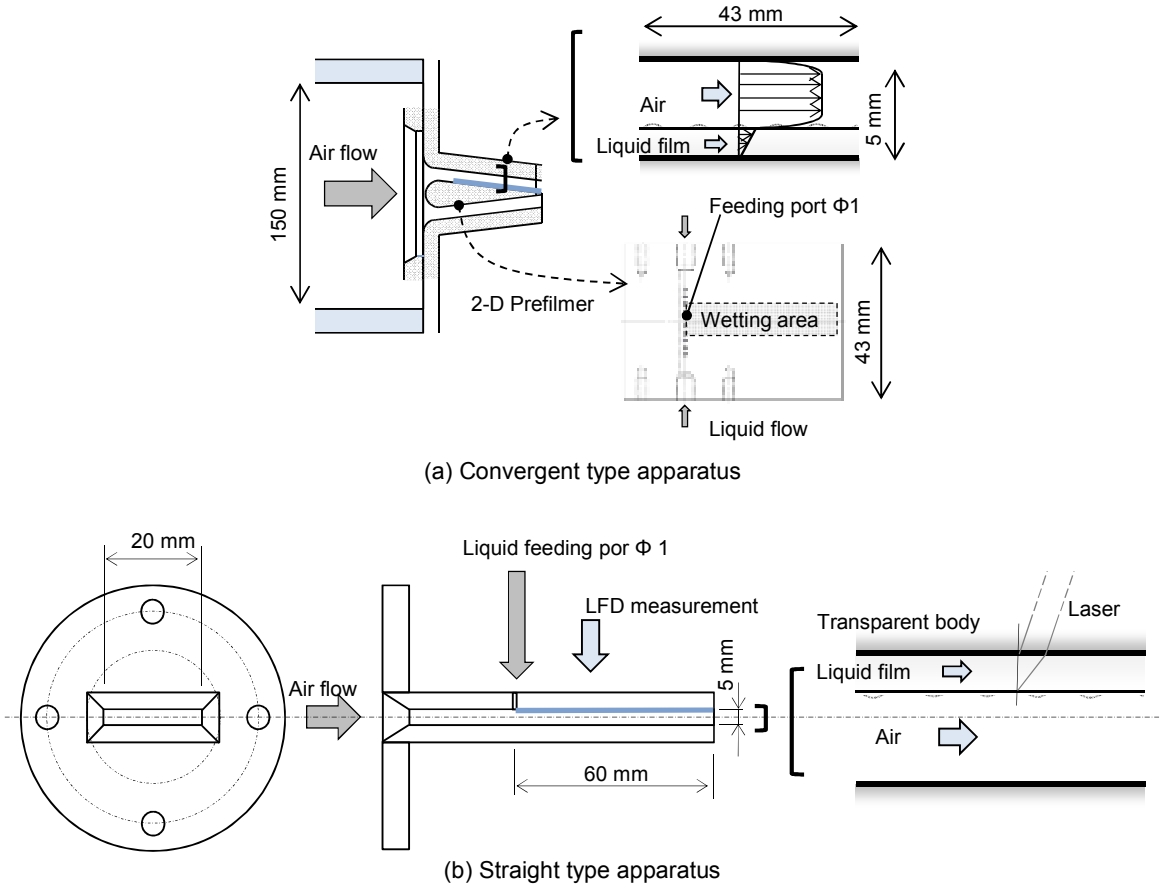

Figure 3. Schematics of two dimensional model apparatuses

In the experiment, the prefilmer of the air-blast atomizer is extracted and two dimensionally modeled for simplicity. Figure 3 shows the schematics of two dimensional model apparatuses. In this study, two kinds of apparatuses are used. Figure 3 (a) shows the convergent type one. This type apparatus is utilized for measurement of the width of the liquid film. The apparatus has convergent air flow channel with rectangular cross section and 2D flat plate that

simulates the prefilmer on the center of the channel. The air that simulates the atomization air flows along the both side of the flat plate. The flat plate also has the same convergent angle as that of flow channel. Therefore the height of the flow passage is constant along the flow direction. The flow passage is 5 mm in height, 45 mm in width. The prefilmer has liquid feeding port on one side of the surface. The feeding port is 1.0 mm in diameter and perpendicular to the surface. The number of the feeding ports is ten and they are equally spaced with 2 mm pitch. The number of the port used is arbitrarily selected in each experiment. The test liquid is fed through the port and thinned onto the surface by the air. The distance from the feeding port to the prefilmer edge is 43 mm. Test liquid is water. The apparatus is made of transparent acryl. The width of the liquid film is measured from direct backlight images obtained by digital single-lens reflex (SLR) camera.

Figure 3 (b) shows the straight type apparatus. This type one is utilized for measurement of the thickness of the liquid film. The apparatus has the flow passage with rectangular cross section. The flow passage is 5 mm in height and 20 mm in width. The liquid feeding port with 1.0 mm in dia. is perpendicularly placed on one surface of the flow passage. The liquid film is formed on the inner surface of the flow passage. Thickness of the liquid film is measured by laser focus displacement meter (LFD) (Keyence LT-9030). The laser is irradiated through the transparent surface of the apparatus and the thickness of the liquid film that is formed on the inner surface of the flow passage is measured. The principle of the LFD measurement and the method of data correction referred in this study are detailed in the previous research [10] done by Takamasa et al. Figure 4 shows the schematic of the experimental system. The prefilmer mentioned above is connected to the air feeding blower. The air is fed and provided to the prefilmer through the air jacket with a straightener. The test liquid is fed by N2 gas pressurizing system. In series of experiments, flow rate, temperature and pressure of the air are measured. Flow rate of the test liquid are also measured. Velocity of the air is calculated from the measurement air flow rate and the cross sectional area of the flow channel.

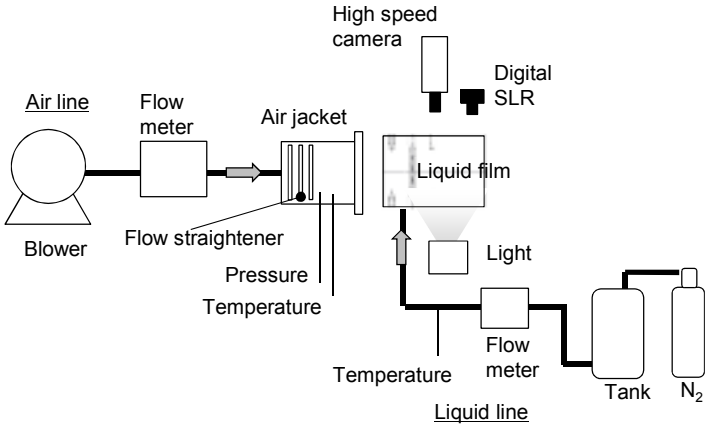

Figure 4. Schematic of experimental system

Result and discussion

Theoretical model validation

Figure 5 shows the typical behavior of the liquid film obtained from the convergent type apparatus. In the figure, the air flows from right to left of the picture. The gravity force acts in downward direction. The number of the port used in this experimental set is ten. Figure 5 (a) shows the result under the condition that the velocity of the air is kept constant and the flow rate of the liquid is varied as a parameter. As can be seen in the figure, the liquid is stretched by the air and makes the uniform liquid film. At 130 cm3/min of liquid flow rate (minimal flow rate in this figure), the liquid makes the separated rivulets immediately on being fed through the ports. The rivulets gradually extend their width and agglomerates with neighboring one in downward region of the prefilmer. The area of the dry regions that is locally observed in the liquid film decreases with increasing liquid flow rate. Un-uniformity in the vertical direction of liquid film is caused by the un-uniformity of the liquid flow rate of each port by the gravity effect. At 270 cm3/min of flow rate (minimal flow rate in this figure), the dry region disappears and the perfectly wetting liquid film is formed over the prefilmer. Figure 5 (b) shows the result under the condition that the liquid flow rate is kept constant and the velocity of the air is varied as a parameter. As a result, the dry region that can be observed in the liquid film decreases with increasing air velocity and makes the perfectly wetting liquid film at the maximal air velocity. This is the same trend as the flow rate parameter case. In this study, the two dimensional wetting behavior is discussed for simplicity. On the

other hand, the prefilmer is cylindrical in practical air-blast nozzle. In the cylindrical prefilmer, the perfectly wet condition is obtained when the total area of the liquid film becomes larger than the area of the prefilmer surface. When this status is obtained, the quantities become uniform in circumferential direction and the number of the unknown quantity in the theoretical modelization is reduced to two. This study focuses on the transient state before the perfectly wet condition is obtained.

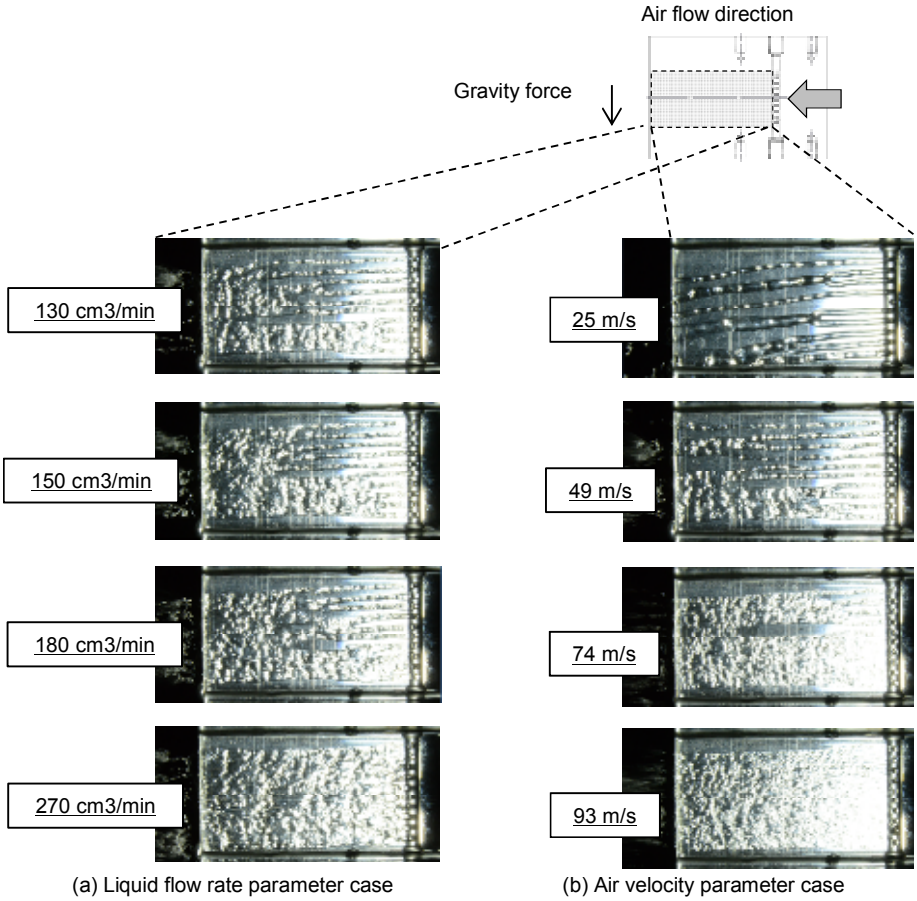

Figure 5. Typical behavior of liquid film in multi feeding port experiment

Figure 6 shows the typical behavior of the single rivulet obtained from the same apparatus. The number of the port used in this experimental set is one. In this condition, the liquid flow rate is kept constant in 20 cm3/min and the velocity of the air is varied from 25 to 93 m/s as a parameter. The flow rate of 20 cm3/min corresponds to the maximal value of the single rivulet experiment in this study. As can be seen in the figure, the rivulet firstly has a curved surface, but becomes thinner film-like shape and its width increases with increasing air velocity. The distribution of the luminosity of the backlight that can be seen on the rivulet is assumed to be due to the difference of the transmissivity caused by the difference of curvature of the surface. So the distribution means the deformation [7] or the instability [8, 11] wave of the film surface, and magnitude of the luminosity has some relationship with the magnitude of the deformation. In the velocity of 25 m/s condition, almost the same scale of the longitudinal waves as the width of the rivulet is formed. In the larger velocity cases, the liquid film becomes wider and the scale of instability waves contrary becomes finer.

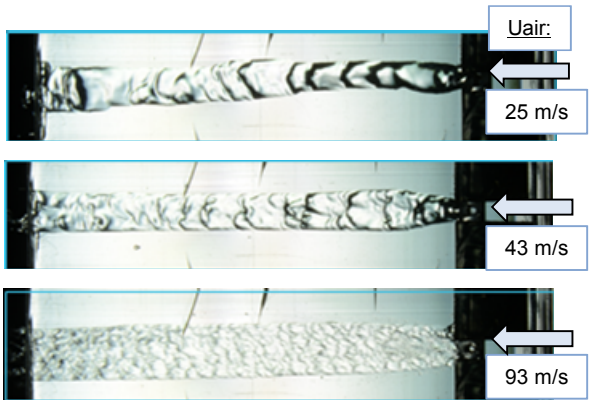

Figure 6. Typical behavior of single liquid rivulet

Figure 7 shows the quantitative measurement of the liquid film width. Figure 7(a) shows the relationship between the liquid film width and the liquid flow rate. In this experimental set, the velocity of the air is kept constant at 43 and 81 m/s and the liquid flow rate is varied as a parameter. As can be seen in the figure, the width of the liquid film uniformly increases with increasing liquid flow rate. In the theoretical model shown in Eq. 10, the width of the liquid film is proportional to the flow rate of the liquid. The lines drawn in the figure show the theoretical dependence of the width of the film on the flow rate. As a result, the theoretical value shows good agreement with the result in both two air velocity conditions. Figure 7(b) shows the relationship between the liquid film width and the air velocity. In this examination, the flow rate of the liquid is kept constant at 5 and 20 cm3/min, and the air velocity is varied as a parameter. As a result, the width of the liquid film uniformly increases with increasing air velocity. This is consistent with the theoretical motion described in Eq. 10 and Eq. 13. The width of the film is proportional to the 2/3 th power of the air velocity in the theoretical model. The curve lines drawn in the figure show the theoretical dependence on the flow rate. As a result, the theoretical value and the results agree well each other.

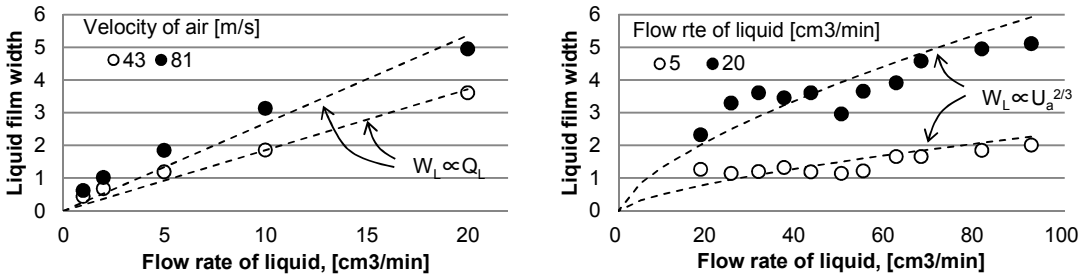

(a) Effect of liquid flow rate on film width

(b) Effect of air velocity on film width

Figure 7. Effect of air condition on width of liquid film

Figure 8 shows the result of thickness measurement of the liquid film by LFD. This result is obtained from the straight type apparatus under the same air velocity and liquid flow rate range as Figure 7. The vertical axis is the thickness. The thickness is the time-averaged value of temporally deformed film by the instability. The horizontal axis is the air velocity. The liquid flow rate is changed as a parameter. As shown in the result, the thickness of the liquid film uniformly decreases with increasing air velocity. The thickness is thinned to be approximately 80 micrometer at maximal air velocity. The curvature drawn in the figure shows the theoretical relationship of the thickness and the velocity obtained from the Eq. 11. The absolute value of the thickness and the tendency of its decrease in the result agree well with theoretical model. The result also shows that the measured thicknesses are slightly different in each flow rate but there is no obvious effect of flow rate; this is consistent with the theoretical model shown in Eq. 11.

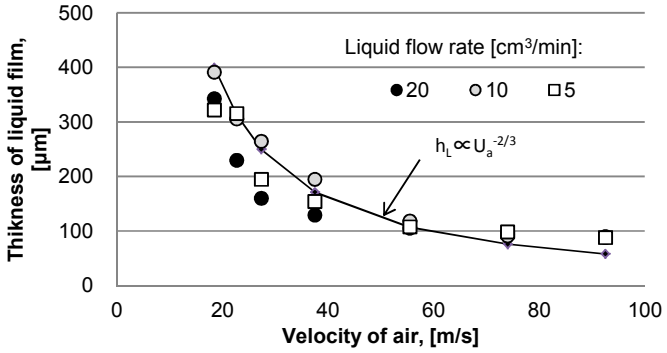

Figure 8. Effect of air velocity on thickness of liquid film

Figure 9 shows the relationship between the theoretical value calculated from Eq. 10 and the experimental value obtained from the convergent type apparatus. The vertical axis of the figure shows the experimental value and the horizontal axis shows the theoretical one. The line drawn in the figure shows the agreement of both values. In this experiment, the liquid flow rate is varied from 1 to 20 mm as a parameter. The velocity of the air is also changed from 25 to 93 m/s in each liquid flow rate condition. As shown in the result, the theoretical value and the experimental one show good agreement with each other in all conditions. The width of the liquid film increases with increasing air velocity in the fixed liquid flow rate condition. In the condition of liquid flow rate of 20 cm3/min, the width of the liquid film changes from 1.8 to 4.3 mm with increasing air velocity. On the other hand, the width at 10 cm3/min changes approximately from 0.9 to 2.2 mm in the same air velocity range; this shows the proportionality of the width to the liquid flow rate. The experimental value is slightly higher than the theoretical one in all condition due to the error of the measurement, experiment or physical property. The magnitude of difference between two values ranges from submilli- to millimeter- order. This indicates the validity of the theoretical model.

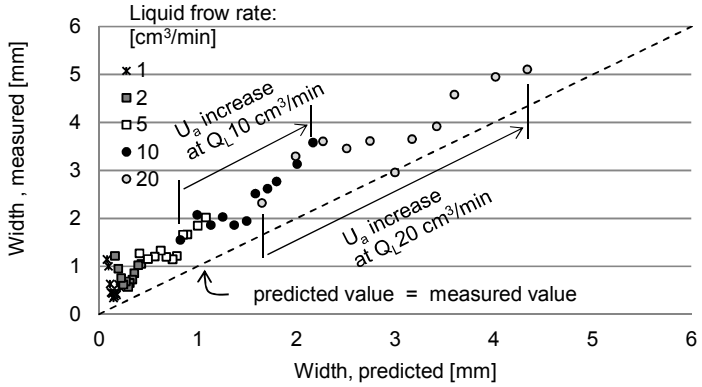

Figure 9. Relationship between theoretically predicted width of liquid film and experimental one

Scale effect on wetting behavior

Here, in below section, the behavior of the liquid film under small liquid flow rate condition, in other wards the small width condition is focused. Figure 10 shows the behavior of the liquid film in small liquid flow rate condition. Figure 10(a) shows the same result as Figure 9, but the both vertical and horizontal axes of the figure are represented as logarithmic scale for detailed observation of the difference. As shown in the result, the difference between the theoretical and experimental values is more apparent with decreasing air velocity in the two smallest flow rate conditions (1 and 2 cm3/min). This characteristic tendency is considered to be derived from distinctly-different causes than the difference observed in larger flow rate conditions. Figure 10(b) shows the behavior of the liquid film in small flow rate condition. This result corresponds to the second-smallest flow rate result in Figure 10 (a). In this condition, the liquid flow rate is kept constant and the velocity of the air is changed from 25 to 93 m/s. In Figure 10(b), the width of the liquid films becomes smaller when the velocity of the air is increased from 25 to 43 m/s. This is inconsistent with the theoretical model. The instability that can be seen apparently in 20 cm3/min of flow rate condition (see Figure 6) is

not observed here. The liquid has a large curvature on its surface and it becomes half-column-like shape rather than a film. When the velocity of the air is increased from 43 to 93 m/s, the liquid flow stretches its width and becomes film-like shape with the instability on its surface.

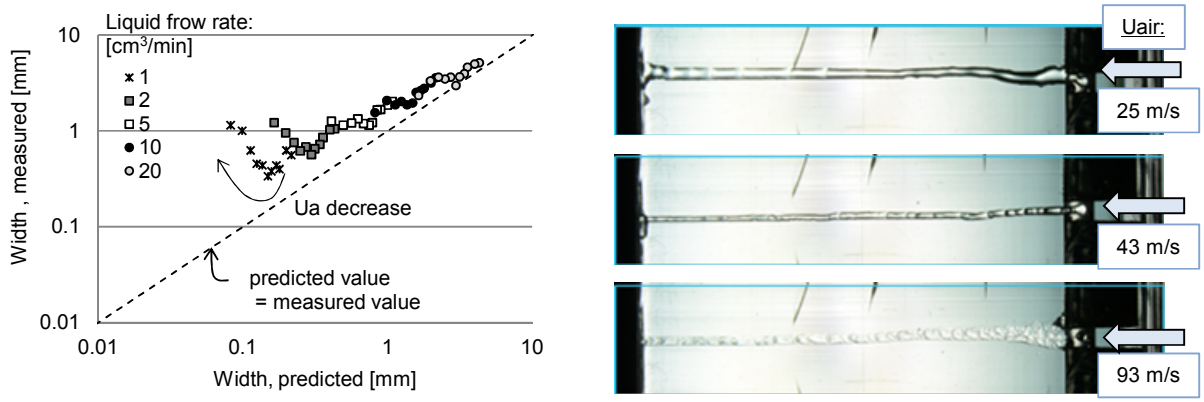

(a) Relationship between predicted width and experimental one (b) Schematic of liquid film

Figure 10. Behavior of liquid film in small liquid flow rate condition

Here, the difference between the theory and the result is discussed from the view point of the scale of the liquid film, in other words, the width of the liquid film caused by the change of the liquid flow rate. In our theoretical model, the shape of the cross section of the liquid film is idealized to be rectangle with adequately large width-to-thickness ratio. On the other hand, the liquid film has finite width and thickness in practical, and it is obvious from Figure 10 (b) that the thickness is varied in each air and liquid flow rate condition. As shown in Eq. 11, the thickness of the liquid film is decided by only the air condition and the physical property of the liquid, and it is independent on the flow rate of the liquid. While, the width of the liquid is proportional to the flow rate of the liquid as shown in Eq. 10. Therefore, the assumption of adequately large width-to-thickness ratio becomes less suitable in smaller liquid flow rate condition under the fixed air velocity condition. In a separate viewpoint, as discussed in the study focusing on the wetting behavior of the liquid film under the condition of strong shear stress or gravity force by Lan et, al [7, 12], the liquid film has deformed shape near its contact line because of the equivalent of the surface tension force and the expanding force by the air. In case the width of the film is much larger, in other words the deformed region is much narrower compared to the overall area of the liquid film, the size of this deformed region is presumed to be constant and independent of its overall width under the constant air condition. When the effect of the deformed region is negligible small, the assumption of rectangular cross section makes sense and the concept of minimal energy in the theoretical model becomes applicable; in other words, minimal energy model is not applicable in case this deformed region is much narrower compared to the overall area of the liquid film. Here, the authors remodelize the motion of the liquid film under the condition that the width of the liquid film is smaller than the scale of the deformed region. Under such conditions, the liquid flow cannot changes its width freely at the minimal energy status but its shape is confined by the surface tension force and other forces. Figure 11 shows the schematic of the remodeled motion of the liquid. The liquid film firstly changes its width freely but be confined its shape by surface tension force with decreasing liquid flow rate. The shape of the liquid in small liquid flow rate is assumed to be a circular arch with the same contact angle as the stable state one for simplicity. The model also assumes the steady Cuette flow profile in any flow-wise cross section. The velocity field of the liquid is not two dimensional and the maximal velocity varies in span-wise direction due to the difference of the thickness. Here, width, height and velocity of the liquid are the quantities to be specified again. The relation of the width and height is uniformly defined by the assumption of the circular arch and contact angle, so that the number of the unknown quantities becomes two. Therefore, the mass and the momentum conservation equations become governing equations to decide the motion of the liquid.

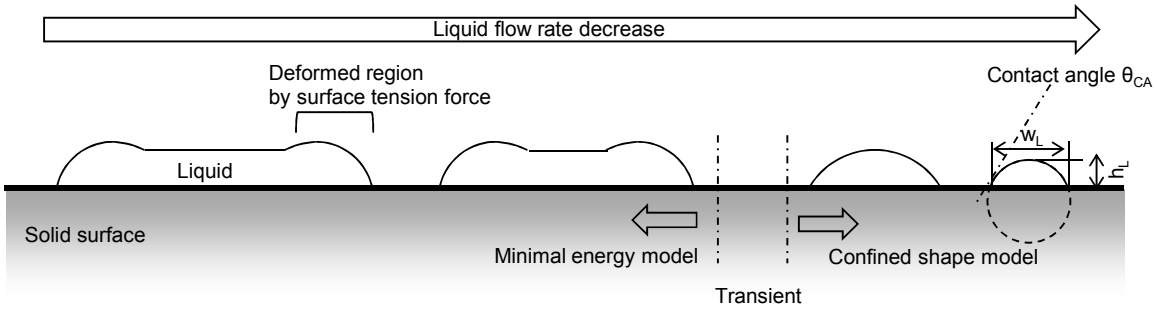

Figure 11. Schematic of modelized motion of liquid flow

From the Cuette flow assumption and the momentum conservation, the velocity of the liquid is obtained as Eq. 14.

$$u_L(x,y)=\left[\frac{\tau_a}{\mu_L}\right] y \tag{14}$$

By integrating the velocity profile of the liquid flow, the mass conservation of the liquid is obtained as Eq. 15.

$$Q_L = \int_{-\frac{w_L}{2}}^{\frac{w_L}{2}} \int_0^{h_L(x)} u_L(x,y)\,dy\,dx \tag{15}$$

The thickness of the liquid along the span-wise direction is represented as Eq. 16. This equation is geometrically obtained from Figure 11 easily.

$$h_L(x)=\left\{\left(\frac{1}{\tan^2\theta_{CA}}+1\right)\left[\frac{w_L}{2}\right]^2 - x^2\right\}^{\frac{1}{2}} - \frac{1}{\tan\theta_{CA}}\left[\frac{w_L}{2}\right] \tag{15}$$

By equating these equations numerically, width, thickness and velocity of the liquid are obtained. Figure 12 shows the width and the thickness of the liquid flow in arbitrary selected conditions. The thickness here means the value at center of the film. Both two values are calculated from the above equations. In this calculation, the flow rate of the liquid is kept constant and the velocity of the air is changed as a parameter. As a result, the thickness of the liquid is uniformly decreases with increasing air velocity. This is the same tendency as the minimal energy model (Eq. 11). On the other hands, the width of the liquid also uniformly decreases with increasing air velocity. This is opposite to Eq. 10 but agrees with the practical motion of the liquid shown in Figure 10. The decrease of the width is caused by the fact that the liquid film has to decrease its cross sectional area with increasing velocity of the liquid due to the increase of the air velocity and constant liquid flow rate condition.

The predicted value obtained from the confined shape model is compared to the one obtained from the minimal energy model and the experimental value. Figure 13 shows the same result as Figure 10, but the predicted value obtained from the confined shape model is added in the figure. The vertical axis shows both the experimental value and the predicted one obtained from the confined shape model. The horizontal axis shows the predicted value obtained from the minimal energy model. The two smallest liquid flow rate cases are shown in the figure. As a result, the experimental value is slightly larger than the confined shape model value but it shows good agreement with the confined shape model rather than the minimal energy one in small air velocity condition. The experimental value is concave up and then approaches asymptotically to the minimal energy value with increasing air velocity. As a result of this study, it is concluded that the liquid film firstly decreases its width with increasing air velocity in accordance with the confined shape model, and then increases its width in accordance with the freely deformed shape model. This effect is apparent in the small flow rate condition due to the small width condition.

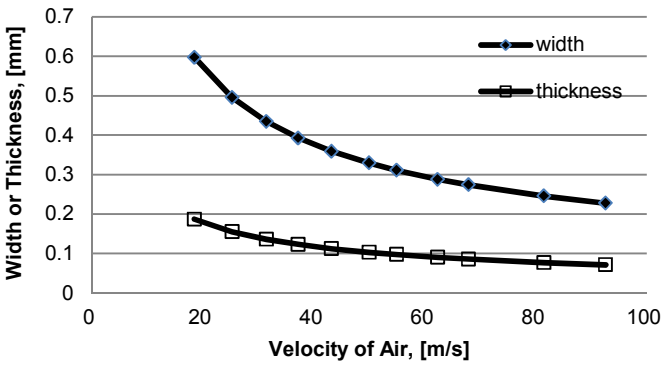

Figure 12. Predicted motion of the liquid flow in confined shape model

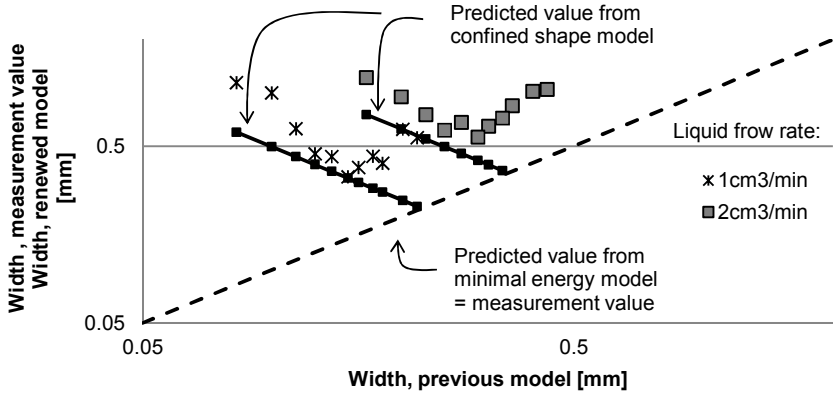

Figure 13. Relationship between predicted width (minimal energy and confined shape) and experimental one

Conclusion

Aiming at the contribution to improve the liquid film formation in the prefilming type air-blast atomizer, this study focuses on the wetting behavior of the finite-width liquid rivulet on the solid surface under the condition of strong shear stress of the air. In this study, the stretching motion of the liquid film is theoretically modeled. The motion of the liquid film is analytically predicted and experimentally validated from the viewpoint of the length scale of the liquid film. The conclusion is following:

The wetting motion of the liquid is theoretically modelized on the basis of minimal energy concept and experimentally validated. In this model, the liquid film freely changes its shape and becomes stable at the minimal energy status. As a result, the theoretical model well predicts the wetting motion of the liquid in much larger liquid flow rate condition, in other wards much larger liquid film width condition. In these conditions, the effect of the influencing factors such as the liquid flow rate and the air velocity on the change of the shape is well consistent with the theoretically predicted one.

On the other hand, the motion of the liquid does not agree with the theoretically predicted one in smaller liquid flow rate condition, in other words smaller liquid film width condition. This is because the assumption of the rectangular cross-sectional shape of the liquid film in the theoretical model becomes less applicable in smaller flow rate condition. In surface tension force-dominant condition due to the small length scale of the liquid, the liquid flow cannot changes its shape freely at the minimal energy status but its shape is geometrically confined by the surface tension force. The confined shape model is theoretically constructed on the basis of the confined shape and compared to the experimental result. As a result, the predicted value agrees well with the experimental value in the small air velocity condition. The width of the liquid is concave up and then approaches asymptotically to the minimal energy value with increasing air velocity.

Nomenclature

c_f	shear stress coefficient [-]
g_p	acceleration [ms^{-2}]
h_L	thickness of liquid film [m]
L	length of parallel to potential direction [m]
Q_L	volumetric flow rate of liquid [$m^3\ s^{-1}$]
u_a	velocity of air [ms^{-1}]
u_L	velocity of liquid [ms^{-1}]
$u_{L,s}$	velocity of liquid film surface [ms^{-1}]
w_L	width of liquid film [m]
x	length in span-wise direction [m]
y	length in thickness-wise direction [m]
ε_{total}	total energy of liquid per unit width [Jm^{-1}]
ε_k	kinetic energy of liquid per unit width [Jm^{-1}]
ε_{st}	surface energy of liquid per unit width [Jm^{-1}]

ε_p potential energy of liquid per unit width [Jm^{-1}]

θ_{CA} contact angle [rad.]

μ_L viscosity coefficient [$P_a s$]

ρ_a density of air [kgm^{-3}]

ρ_L density of liquid [kgm^{-3}]

σ_{LV} surface tension coefficient liquid-gas [Nm^{-1}]

σ_{LS} surface tension coefficient solid-liquid [Nm^{-1}]

σ_{SV} surface tension coefficient gas-solid [Nm^{-1}]

τ_a shear stress of air [P_a]

References

[1] Lefebvre, A.H. and Ballal D. R., 2010, "Gas Turbine Combustion Third Edition."
[2] Lefebvre, A.H., 1989, "Atomization and Sprays."
[3] Nasser, A., 2011, "Handbook of Atomization and Sprays."
[4] Rizk , N. K. and Lefebvre, A. H., 1980, Journal of Engineering for Power, 102, pp. 706-710.
[5] Monnier, H., Mhiri, N and Falk, L., 2010, Chemical Engineering and Processing, 49, pp. 953-957.
[6] Witting, S., et al., 1992, Journal of Engineering for Gas Turbines and Power, 114, pp. 395-400.
[7] Lan, H., et al., 2010, Journal of Fluids Engineering, 132, 081301(8 pages),.
[8] Inamura, T., et al., Sep. 2.-6. 2012, 12th International Conference on Liquid Atomization and Spray Systems.
[9] Leger, L. and Joanny, J. F., 1992, Reports on Progress in Physics, 55, pp. 431-486,.
[10] Takamasa, T. and Hazuku, T., 2000, International Journal of Heat and Mass Transfer, 43, pp. 2807-2819
[11] Aliseda, A., et al., 2008, International Journal of Multiphase Flow, 34, pp. 161–175.
[12] Lan, H., et al., 2008, International Journal of Heat and Fluid Flow, 29, pp. 449–459.